SINTEF A184 - Unrestricted

REPORT

Prediction errors associated with sparse grid estimates of local atmospheric flows

Karl J. Eidsvik

SINTEF ICT
Applied Mathematics

June 2006

SINTEF

SINTEF ICT

Address: NO-7465 Trondheim, NORWAY
Location: Alfred Getz vei 1, NTNU NO-7491 Trondheim
Telephone: +47 73 59 30 48
Fax: +47 73 59 29 71

Enterprise No.: NO 948 007 029 MVA

SINTEF REPORT

TITLE

Prediction errors associated with sparse grid estimates of local atmospheric flows

AUTHOR(S)

Karl J. Eidsvik

CLIENT(S)

Avinor AS

REPORT NO.	CLASSIFICATION	CLIENTS REF.	
SINTEF A184	Unrestricted	Erling Bergersen	
CLASS. THIS PAGE	ISBN	PROJECT NO.	NO. OF PAGES/APPENDICES
Unrestricted	82-14-04027-2	90A260	20
ELECTRONIC FILE CODE		PROJECT MANAGER (NAME, SIGN.)	CHECKED BY (NAME, SIGN.)
SINTEF A184.pdf		Karl J. Eidsvik K. J. Eidsvik	Karstein Sørli K. Sørli
FILE CODE	DATE	APPROVED BY (NAME, POSITION, SIGN.)	
90A260	2006-06-20	for Svein Nordenson, Research Director Runar Holdahl	

ABSTRACT

Numerical simulations of geophysical flows have to be done on very sparse grids. This study show that moderately stratified flows can nevertheless be predicted usefully accurate. For better grids than about $\Delta x_1/H \sim 0.5$ or so, recirculating domains and the characteristic wavelength of lee waves are predicted accurately while the lee wave amplitude is predicted with considerable error. The relative error of the turbulence intensity is comparable to $\delta\sqrt{K}/\sqrt{K} \sim 0.25$, which is comparable to the large scale flow error and the about as accurate as any turbulence model can be. Strongly stratified flows are predicted with considerable errors even on dense grids.

KEYWORDS	ENGLISH	NORWEGIAN
GROUP 1	Meteorology	Meteorologi
GROUP 2	Turbulence	Turbulens
SELECTED BY AUTHOR	Flight safety	Flysikkerhet

PREDICTION ERRORS ASSOCIATED WITH SPARSE GRID ESTIMATES OF LOCAL ATMOSPHERIC FLOWS

Eidsvik K.J.
SINTEF Applied Mathematics.
N-7465 Trondheim, Norway.

June 20, 2006

1 Introduction

A prediction system for the local flow in mountainous terrain is developed (Utnes 2002, Lie et al 2003, Eidsvik et al 2004, Eidsvik 2005). The prediction is based upon synoptic scale information, which is downscaled by means of detailed information about the terrain and fully three-dimensional flow models (Figure 1). Although all models integrate efficiently parallel, the time-step constraint: $\triangle t < \triangle x_1/U$ makes high-resolution estimations expensive. As for all meteorological prediction models, the gridding therefore have to be sparse, even in the most local model of a system like in Figure 1. This study estimate errors associated with too sparse gridding of the most local model, given that the larger scale flow is known.

For the purpose of comparison, the prediction error of the large scale flow (UM1-scale) should also be estimated, but quantitative estimates of errors associated with meteorological predictions are scarce. For the purpose of this study a large scale weakly stratified flow is represented with the flow near the top of the boundary layer: U. Very roughly its prediction error should be comparable to the structure function for horizontal velocity components. For scales between about 10^2Km and 10^3Km, corresponding to timescales between about 2hr and 24hr, where two-dimensional (geostropic) turbulence is dominant, the relative error is then very roughly: $\delta U/U \sim 0.2(f\triangle t) \sim 0.2$, where $f \approx 10^{-4}s^{-1}$ is the Coriolis parameter and $\triangle t \sim$5 hr. is the lead time for the prediction (Lindborg and Cho 2001, with references therein). The total relative prediction error for the mean value , $u_i =< u_i >$, and standard deviation of a velocity component (characteristic turbulent velocity, turbulent kinetic energy) $\sigma_i \sim u_t \sim \sqrt{K}$, can be roughly estimated from relations like: $u_i = (u_i/U)U$, as: $\delta u_i/u_i \sim \delta(u_i/U)/(u_i/U) + \delta U/U$. The first term on the right hand side represents the prediction error given that the larger scale flow is known, and only this is estimated here. When misunderstandings are not probable, the normalization with U may then be neglected. Preferrably this error should not be significantly larger than the larger scale error: $\delta U/U \sim$0.2.

The simplest error associated with too sparse gridding is that the terrain height and slope can be seriously underestimated. Suppose that a hill is characterized by its maximum heigt: H=O(500m), and halve-width: L=O(2Km), relative to the surrounding terrain. For resolving the maximum height the grid resolution have to be better than about $\triangle x_1/L <$0.3. Since the terrain slope, comparable to: H/L, is a spatial derivative, it focus small scale variations even more so that it may be significantly underestimated on a sparse grid. The predicted flow may then be attached when in reality it should have been separated, for about H/L>0.5, corresponding to 25 degrees. The wind-shear and turbulent intensity may therefore be seriously underestimated. Even for less dramatic differences the turbulent intensity may be underestimated on sparse grids.

This is so because the turbulent production is proportional to the mean wind shear squared: $P \approx u_t l_t (\partial u_i/\partial x_j)^2$, so that the spectrum of energy production is focused towards the small scale variations which cannot be represented realistically if the grid is too sparse.

The relatively unknown surface properties also gives flow estimation errors. Even the surface roughness distribution over a given terrain is quite unknown. Also the local thermodynamic forcing depends significantly upon the surface properties. For instance, as the system (Figure 1) functions presently, the regional scale cooling during clear nights appears to overestimate the turbidity flows from the valleys. The stratification associated with such flows may then decouple the low level flow from the large scale flow over the mountains so that the latter flow do not "see" the actual terrain. This means that the low level flow may be quite independent of the upper layer flow, making the downscaling procedure (Figure 1) inaccurate (Eidsvik et al 2004).

Stratified flows with $N^2 = (g/\theta)\partial\theta/\partial x_3 > 0$, are associated with lee waves, rotors, breaking waves, hydraulic transitions, vortex wakes, ship waves and bifurcations (Baines 1995, Wurtele et al 1996), so that the flow over a given local terrain may be critically dependent upon the detailed history of the flow over the regional scale terrain. Therefore these features should also be predicted accurately on the regional scale. The gridding of the regional scale model can probably not be sufficiently dense for this, but it is hoped that the general properties of lee waves with characteristic wavelength $\lambda \sim 2\pi U/N$ =O(5Km) (Baines 1995) and moderate amplitudes should be represented reasonably accurately also in the regional scale model. It is also hoped that the information about lee waves on the regional scale grid can be transformed accurately to the more detailed local scale grid. However, problems with downscaling internal wave flows will only be addressed implicitly in this study. Convective flows, $\partial\theta/\partial x_3 < 0$, with cumulus clouds, have energetic coherent eddies with spatial scales as small as 100m (Emanuel 1994). In a coordinate system moving with the mean flow the most local model can simulate such flows, but the prediction system (Figure 1) can not. Convective effects are only parameterized in the simplest manner, so that errors associated with convection will not be discussed.

Again: the purpose of this study is to investigate if the standard local model in Figure 1, which is reasonably realistic on sufficiently dense grids, can also predict usefully accurate on very sparse grids. The focus is towards errors that are most relevant for estimating the flying safety, the wind shear and turbulence. With intense turbulence the turbulent standard deviation, $\sigma_i \sim u_t \sim \sqrt{K}$ is most important for both (Eidsvik et al 2004).

Since the prediction system should be applicable in most interesting flows, the gridding error is estimated roughly in several idealized flows. The vertical-, $\triangle x_3/H$ and horizontal gridding, $\triangle x_1/L$, $\triangle x_2/L$, are chosen to be approximately proportional so that they can be represented roughly with $\triangle x_1/H$.

It turns out that moderately stratified flows are predicted usefully accurate in terms of resirculation domains and characteristic wavelength for lee waves even on quite sparse grids. The lee wave amplitude is predicted less accurately. For better grids than about $\triangle x_1/H$ <0.5 or so, the relative error $\delta\sqrt{K}/\sqrt{K}$ is smaller than about 0.25, which is comparable to the large scale error and about as accurate as any turbulence model can be. For flows with resirculation domains, it also turns out that this error is systematic in that sparse gridding underestimates the turbulent intensity. This may be used for corrections of the sparse grid estimates from the prediction system (Figure 1).

For strongly stratified flows with hydraulic transitions, it appears that the turbulence model underestimates the turbulent intensity seriously. Although such flows are dramatic, for moderate hill height they are associated with small U-values, so that this error may not be very important for flight safety.

2 Simple Modelling of Geophysical Turbulence

The HIRLAM, UM and SIMRA numerical models (Figure 1) are based first principles like the conservation of mean momentum, mass and potential temperature (Pope 2000, Eidsvik et al 2004). A rational turbulence model for stratified geophysical flows with energetic quasi-horizontal, an-isotropic large scale eddies is not available (Phanofsky and Dutton 1984, Kaimal and Finnigan 1994). In a system like in Figure 1 the integration speed and robustness are so essential that many-equation models cannot be afforded (Brørs and Eidsvik 1992, 1994, Hewitt and Vassilicos 2005). Therefore, until a rational turbulence model for stratified geophysical flows is documented, the most standard few-equation model from laboratory scale flows are applied. The turbulent stress is estimated from the Boussinesq viscosity approximation. with a turbulent viscosity coefficient given as $\nu_t = u_t l_t$, where the turbulent velocity and length-scale are $u_t = (C_\mu^{1/2} K)^{1/2}$ and $l_t \approx u_t^3/\epsilon$ respectively. The turbulent kinetic energy and dissipation ϵ, are estimated dynamically from Equations 1 and 2. Here $P = - < u_i^{'} u_j^{'} > \partial u_i/\partial x_j$, and $G =< \theta^{'} u_3^{'} > g/\theta$. Adjustments of the standard coefficient may commonly make predictions by standard models apparently better when applied to geophysical flows, but since such curve-fits may not be related to model accuracy, standard coefficients are applied here, $(\kappa, C_\mu, C_{\epsilon 1}, C_{\epsilon 2}, C_{\epsilon 3}, \sigma_K, \sigma_\epsilon) = (0.41, 0.09, 1.92, 1.43, 1, 1, 1.3)$, (Pope 2000).

$$\frac{\partial K}{\partial t} + \frac{\partial}{\partial x_j} K u_j = P + G - \epsilon - \frac{\partial}{\partial x_j} < K^{'} u_j^{'} > \tag{1}$$

$$\frac{\partial \epsilon}{\partial t} + \frac{\partial}{\partial x_j} \epsilon u_j = (C_{\epsilon 1} P + C_{\epsilon 3} G - C_{\epsilon 2} \epsilon) \frac{< \epsilon >}{< K >} - \frac{\partial}{\partial x_j} < \epsilon^{'} u_j^{'} > \tag{2}$$

The available evidence suggests that this model is also usefully accurate for moderately stratified geophysical flows. However, K and ϵ as estimated from Equations 1, 2, should then be interpreted so that the quasi-horizontal, an-isotropic large scale eddies can also be estimated. For the purpose of this study, we feel that it is rational to extrapolate from what is most commonly accepted both for laboratory- and full scale geophysical flows, the structure of the smallest isotropic inertial subrange eddies:

The energy dissipation $\epsilon = \nu(\partial u_i^{'}/\partial x_j)^2$, really occurs near the Kolmogorov micro-scale, but in Equation 2 it is rather to be interpreted as the inertial subrange energy transfer from the large to smaller eddies. It also measures the intensity of the inertial subrange spectrum and the associated covariance $Q_{ij}(\triangle \mathbf{x}) =< u_i^{'}(\mathbf{x}) u_j^{'}(\mathbf{x} + \triangle \mathbf{x}) >$ function (Pope 2000). The dissipation can also be interpreted as the characteristic length-scale of the most energetic quasi-isotropic, but also flux-containing turbulent eddies. This length-scale should therefore be representative for the vertical velocity component both in laboratory scale and geophysical flows.

The turbulent kinetic energy K as estimated from Equation 1, is supposed to contain energy from the quasi-isotropic and flux-containing eddies. Even the largest of the eddies associated with significant vertical velocity, contributing most to vertical fluxes $< u_i^{'} u_3^{'} >$, $< K^{'} u_3^{'} >$ and the wall stress $u_*^2 \approx C_\mu^{1/2} K(x_3 \rightarrow 0)$ are supposed to be included in the estimated K. It therefore follows that $K \approx 3/2 Q_{33}$. The spectrum of the vertical velocity component can be roughly approximated with the Kaimal model spectrum (Equation 3 with $l_{t3} = l_t$).

$$k_1 E_{ii}(k_1) \approx \frac{Q_{ii}(0) k_1/k_{mi}}{[1 + (3/2)(k_1/k_{mi})]^{5/3}}, \qquad l_{ti} k_{mi} \approx \frac{4}{3} (\frac{3}{2})^{5/2} (\frac{\alpha_K C_\mu^{1/2} K}{Q_{ii}(0)})^{3/2} \qquad i > 1 \tag{3}$$

$$\frac{\sigma_1}{\sigma_3} = (\frac{Q_{11}(0)}{Q_{33}(0)})^{1/2} \sim (\frac{3}{4})^{1/2} (\frac{l_{t1}}{l_{t3}})^{1/3} \tag{4}$$

The largest scale quasi-horizontal, an-isotropic geophysical eddies are supposed not to be contained in K and ϵ as estimated from Equations 1 and 2, but it may still be convenient to include them in what we call "turbulence". These fluctuations must be estimated by means of ad hoc relations. Experimental evidence from the near bottom equilibrium boundary layer over flat land suggest that the variance of $u_i^{'}$ is related to $K \approx C_\mu^{-1/2} u_*^2$, like: $Q_{11}(0) \approx Q_{22}(0) \approx 4.5u_*^2 \approx 1.4K$, $Q_{33}(0) \approx 1.7u_*^2 \approx 0.5K \sim (2/3)K$ (Phanofsky and Dutton 1984, Kaimal and Finnigan 1994, Utnes and Eidsvik 1996). This means that $\sigma_1/\sigma_3 \sim 1.7$ or so. Very approximately the Kaimal spectrum (Equation 3 and 4) is also fruitful for the horizontal velocity components and temperature, so that the σ_1/σ_3-ratio of 1.7 corresponds to $l_{t1}/l_{t3} \sim 7.0$ (Equation 4). Other data suggest that the one-dimensional spectra for the horizontal velocity components and temperature tend to follow -5/3 spectral laws even farther beyond $k_{m3} \sim 1/l_{t3}$, say to $k_{m1} \sim 1/l_{t1} \sim 1/l_{t2} \sim 1/D \approx 1/1Km$ (Panofsky and Dutton 1984, Kaimal and Finnigan 1994). For long time averages of larger scale two-dimensional turbulence this spectral law is even estimated up to about $l_{t1} \sim$100Km (Lindborg and Cho 2001).

Since the large scale contribution is supposed to be associated with small vertical velocity, it contribute little to vertical fluxes and wall stress, so it may not be dynamically essential. This is one reason why there may be some hope that a standard turbulence model developed and tuned to laboratory-scale flows, may be useful also to weakly stratified full-scale geophysical flows.

3 Simulations

3.1 Inflow Profiles

For the purpose of this study the incoming flow at the "west" boundary of SIMRA is approximated as in Equation 5 (Panofsky and Dutton 1985, Kaimal and Finnigan 1994). The friction velocity is u_* and the stratification is supposed to affect the flow negligibly. The wake function can be approximated as $W(x_3/D) = (A-1)(x_3/D) - A/2(x_3/D)^2$ which behaves properly as $x_3/D = 1$, regardless of the coefficient choice ($A \approx 4$).

$$u_0(x_3) \approx \frac{u_*}{\kappa}(ln\frac{x_3}{z_0} + W(\frac{x_3}{D})) \tag{5}$$

The turbulent lengthscale-, kinetic energy- and dissipation profiles at the "west" boundary are estimated as $1/l_t(x_3) \approx 1/\kappa x_3 + 1/\kappa D$, $\epsilon(x_3) \approx (C_\mu^{1/4} K(x_3)^{1/2})^3/l_t(x_3)$, with:

$$C_\mu^{1/2} K_0(x_3) \approx - < u_1^{'} u_3^{'} > (x_3) \approx l_t(x_3)^2 |\frac{du_0(x_3)}{dx_3}|^2 \approx u_*^2(1 - \frac{x_3}{D})^2 \tag{6}$$

In neutrally stratified flows the Ekman layer thickness is: $D \approx 0.2u_*/f = O(1km)$, but for stratified flows a neutral surface boundary layer is normally capped by a potential temperature interface $\triangle\theta = \theta(D) - \theta(0)$, at $x_3 = D$, with a fairly constant Brunt Vaisila frequency: $N^2 = (g/\Theta)(\partial\Theta/\partial x_3)$ above:

$$\theta(x_3) = \theta(0), \quad for \quad x_3 < D$$

$$\theta(x_3) = \theta(D) + \frac{\partial\theta}{\partial x_3}(x_3 - D) = \theta(D)[1 + \frac{N^2}{g}(x_3 - D)], \quad for \quad x_3 > D \tag{7}$$

If a flow like above with initial $D \approx 0$ is heated and mixed from below, D and the potential temperature jump will increase with time like: $\triangle\theta \approx (\partial\theta/\partial x_3)D = (\theta(0)/g)N^2 D$, so that the relative internal wave speed and Froude number are: $c_r^2 = (\triangle\theta/\theta(0))gD = (ND)^2$, and $U/c_r = U/ND$.

With stationary inflow, it is expected that the simulated flows should also be stationary. However, it turns out that some dynamics remains even after quite long integration times. The simulation results to be illustrated contain such variations, but their relative magnitude are significantly smaller than the errors associated with the coarse gridding.

3.2 Attached Flow over a Hill

Neutrally stratified attached flow over a hill is studied with reference to the Askervein hill experiments . The maximum slope is about H/L$\approx$ 0.5, corresponding to 25 degrees, which is marginal for attached flow. These data are one of the most classic references for validating models for geophysical flows, and several models can be adjusted to "predict" these data very accurately even on very sparse grids. Castro et al (2005) concludes that grids comparable to $N_1 \times N_2 \times N_3 \sim 50 \times 50 \times 30$, with near ground vertical resolution comparable to: $\triangle x_3/z_0 \sim$20, $z_0 \approx$0.03m are sufficient. Castro et al (2005) apply a (K, ϵ)- turbulence model with a nonstandard turbulent viscosity, (C_μ=0.033 instead of C_μ= 0.09). Also standard turbulence models predicts these data quite accurately on sparse grids. The SIMRA model, with a standard Gatski- Speziale (1993) algebraic turbulence closure, do so (Eidsvik 2005) and Figure 2 illustrates that also the standard (K, ϵ)- turbulence model with standard coefficients do (compare Figure 2a with Eidsvik 2005). Even the general variation of the turbulence, $\triangle K/K_0$, along the terrain, with the rapid increase behind the hill-crest is predicted quite accurately on quite sparse grids. A main reason for this sparse grid accuracy may be that this flow is governed by the Jackson-Hunt (1975) speedup effects, where the main flow gradients are normal to the terrain. A reasonably accurate representation along this direction is sufficient for a quite accurate prediction of the whole flow.

However, Figure 2a suggests an unexpected grid variation in that the simulation on the most detailed grids appear to give the largest velocity defect "errors" behind the hill. Since Figure 3b illustrate that $\triangle u/u_0$ vary quite much over small distances along the hillside in this area, with a minimum value smaller than $\triangle u/u_0 \sim$-0.8, these differences may not be significant. Also, since the mean flow and turbulence is estimated as: $u \approx 4.0$ m/s and $\sqrt{K} \approx 2.5$m/s in this area, the relative accuracy of these $\triangle u/u_0$-data may be quite large, say 0.5 or so. Both arguments suggest that the differences between the $\triangle u/u_0$-data and fine grid predictions may not be significant.

But also the variations of $\triangle K/K_0$ appear to suggest that the prediction error behind the hill may not decrease with increasing grid resolution (Figure 2b), and Figure 3b illustrate that $\triangle K/K_0$ for the best grid is systematically too small in this area, say smaller than $\triangle K/K_0 \sim$1.5 or so. From Figure 2b we estimate that the predicted near wall turbulence is associated with a relative error of $\triangle K/K_0$ as large as 0.5 or so, over the whole hill. Equation 8 then illustrates that the relative error of $\sqrt{K}$ is only about halve as large as the relative error of $\triangle K/K_0$, say about 0.25, and this is comparable to the accuracy of most turbulence closures which are models and not curve-fits. The inaccuracy of the turbulence predictions should therefore be accepted as moderate, particularly so when this is geophysical turbulence.

$$\sqrt{K} = \sqrt{K_0[1 + \frac{\triangle K}{K_0}]} \tag{8}$$

In summary: the differences between the predictions and the data are therefore considered to be moderate and a better gridding than, say $\triangle x_1/H <$0.6 is estimated as sufficient for predicting such flows usefully accurately, also in terms of the turbulent intensity.

3.3 Separated flows over idealized Hills

Separated flows over hills are studied with reference to Hunt and Snyder's (1980) laboratory scale experiments, with an axisymmetric hill with D/H=0.3 and z_0/H=0.00033. We simu-

late large Reynolds number geophysical flows and upscale the parameters from H=0.229m to H=500m. For the purpose of obtaining simpler understanding and denser numerical resolution, two-dimensional simulations over a cosine-square hill with L/H =2 is also simulated (Utnes and Eidsvik 1996). Since the separation is more important than the details of the incoming flow, the predictions are now discussed in terms of u_i/U and $\sqrt{K}/U$ rather than in terms of $\triangle u_i/U$ and $\triangle K/K_0$.

Figure 4 and 5, can be compared with Hunt and Snyder's (1980) Figure 15e. The details of the small scale variations near a complicated hilltop like this can obviously not be predicted accurately on sparse grids. Nevertheless the larger scale variations are so and for the purpose of this study the predicted flow corresponds well to the data. Both the main separation point at about $(x_1, x_2) \approx$ (0.6, 0) and the reattachment point $(x_1, x_2) \approx$ (3.5, 0) (Hunt and Snyder 1980) are predicted quite similar. Also the width of the main recirculation area are similar to the data, recirculation defined as the domain with negative u_1-component. Turbulence was not measured, but in a recirculating flow like this the maximum turbulence intensity should be close to: $\sqrt{K}/U \approx$0.25 (Rodi and Bonnin 1997), like suggested by the simulations.

The grid dependence is illustrated in Figure 6, and a systematic increase of the reattachment distance with increasing grid resolution is estimated, like in the classical backward facing step flow (Pope 2000, Hewitt and Vassilicos 2005). Also the estimated maximum turbulent intensity, $\sqrt{K}/U$ tend to increase with increasing grid resolution, as expected.

The two-dimensional flow is experimentally verified to be similar to the classical flow over a backward facing step, with a reattachment distance and maximum turbulent intensity comparable to $x_r/H \approx 6.5$ and $\sqrt{K}/U \approx$0.25 (Rodi and Bonnin 1995, Utnes and Eidsvik 1996) and also Figure 7 illustrate that this is so. The flow is estimated to separate slightly behind the hill-crest, leaving a thin shear layer trailing behind. The thickness of this shear layer turns out to be quite grid dependent and the vorticity distribution in Figure 7 suggests that even the most detailed grid applied here is not dense enough to represent this shear layer very accurately. As for the backward facing step flow, the reattachment point and the maximum turbulent intensity must also be expected to converge slowly towards the correct values, and Figure 8 illustrate this. Nevertheless, the bulk properties of the flow are predicted plausibly, even on sparse grids.

In summary: the simulations suggest that even a gridding as coarse as about $\triangle x_1/H \sim$0.6 give usefully accurate predictions of complicated massively separated flows. However, both the reattachment distance and maximum turbulent intensity are underestimated, as illustrated in the Figures 6 and 8. For steep hills it should be recalled that $\triangle x_1/L$ is also supposed to be sufficiently small so that a separation can be represented.

3.4 Stratified wave flows over idealized Hills

Stratified flows are also studied with reference to Hunt and Snyder's (1980) laboratory scale experiments. The inflow profile of density (potential temperature) is like in Equation 7, without a density interface. What Baines (1995) calls the inverse steepness number: U/NH, is varied over $0.1 < U/NH < 1.7$. Two-dimensional stratified flows are studied with reference to Vosper (2004) and Sheridan and Vosper (2005). The flow is estimated to be governed by the non-dimensional numbers: U/c_r, U/ND, D/H . When the inversion is generated by convection like suggested below Equation 7, so that: c_r=ND, there are only two independent numbers. Sheridan and Vosper (2005) find that lee waves can occur when: $(U/c_r)^2 < Tanh(ND/U)/(ND/U) \sim [1 - (1/3)(U/ND)^{-2}] \sim 1$. For $D/H > 2.5$ the lee waves have moderate amplitudes. For $D/H < 2.5$ and $0.4 < U/c_r < 1$ the lee waves have large amplitudes with rotors and for U/c_r <0.4 there is an hydraulic jump behind the mountain with small lee wave amplitudes. The characteristic wavelength of the lee waves is estimated as in Equations 9 and 10 (Hunt and

Snyder 1980, Baines 1995, Vosper 2004).

$$\frac{\lambda}{2\pi H} \approx \frac{U}{NH}, \qquad for \qquad \frac{D}{H} << 1 \tag{9}$$

$$\frac{\lambda}{2\pi D} \approx 2[(\frac{U}{c_r}\frac{ND}{U})^2 + (\frac{U}{c_r})^{-2}]^{-1} \sim 2[1 + (\frac{U}{c_r})^{-2}]^{-1} \sim \frac{U}{c_r}, \qquad for \qquad \frac{D}{H} = O(1) \tag{10}$$

A necessary grid requirement for representing lee waves like this is that the resolution should be significantly better than the Nyquist condition: $\triangle x_1 < \lambda/2$. In the lee wave region, $U/NH = O(1)$, $0.4 < U/c_r < 1$, this gives approximately:

$$\frac{\triangle x_1}{H} < Min[\pi(\frac{U}{NH}), 2\pi\frac{D}{H}[1 + (\frac{U}{c_r})^{-2}]^{-1}] \sim 3.0 \tag{11}$$

Hunt and Snyder's (1980) U/NH=0.8- flow is illustrated in the Figures 9 and 10. As expected from data (Hunt and Snyder 1980, Baines 1995) it is predicted to be attached over the hill, with well developed lee waves. The characteristic lee wavelength, estimated as about λ/H ≈5.0, is similar to the linear estimate in Equation 9. Also the low level rotor flow is realistic. Although the maximum turbulent intensity in the rotor flow is estimated as almost $\sqrt{K}/U$ ∼0.2, this may be considerable to small relative to common conceptions of rotor flows. As have been experienced before, the stratification do probably damp the (K, ϵ) turbulence too much (Brørs and Eidsvik 1992, 1994, Hewitt and Vassilicos 2005).

The grid dependence of the characteristic lee wavelength, maximum wave vertical velocity and maximum rotor turbulent intensity are illustrated in Figure 11. It appears that the correct lee wavelength is estimated as soon as the lee waves are resolved reasonably well. However, the lee wave amplitude as characterized with the maximum vertical velocity increases systematically with the grid resolution. The maximum turbulent intensity also increases systematically with the grid resolution, but as mentioned, it is probably significantly underestimated even on a very dense grid.

A two-dimensional wave flow is estimated in Figure 12. In agreement with Sheridan and Vosper (2005) the parameters D/H=1.4 and U/c_r ≈0.67 (corresponding to U/NH=0.9), are consistent with significant lee waves and rotors. The grid dependence of the numerical solution is estimated in Figure 13. Firstly, the dominant linear wavelength λ/H ≈5.5 (Equation 10), is estimated within the estimation uncertainty, say $\triangle\lambda/H$ ∼0.5 (Subjectively judged from figures like 12), even on the coarsest grids. The wave amplitude, in terms of the characteristic maximum wave vertical velocity is reduced considerably with decreasing grid resolution. As for the neutrally stratified flow, the maximum turbulent intensity is also systematically underestimated on coarse grids.

In summary: the Figures 11 and 13 suggest that better grids than about $\triangle x_1/H$ ∼0.5 or so, give quite realistic predictions of lee wave flows with low level rotors. However, the wave amplitude and maximum turbulent intensity are systematically underestimated. It should be recalled that $\triangle x_1/L$ is also supposed to be sufficiently small, say $\triangle x_1/L$ <0.25 so that the difference between a separation and a downslope jet can be represented.

3.5 Flows with hydraulic Transition

Strongly stratified flows are also studied with reference to Hunt and Snyder's (1980) laboratory scale experiments and Sheridan and Vosper's (2005) simulations. Figure 14 and 15 illustrate the predicted U/NH=0.4- flow, to be compared with Hunt and Snyder's (1980) Figure 15b. The predicted speedup down the lee slope, with the hydraulic transition are evident. The transition point $(x_1, x_2)/H \approx (1.0, 0)$ (Hunt and Snyder 1980), is predicted quite well but the reattachment

point $(x_1, x_2)/H \approx$ (3.0, 0) is predicted to be larger than (6.0, 0). Also the width of the wake area seems to be over-predicted. The several isolines in the wake area are insignificant, all for small and similar values. The characteristic scale for the variations downstream of the transition corresponds to the characteristic lee wavelength (Equation 9, Figure 15).

Again the turbulence was not measured by Hunt and Snyder (1980), but the common conception that hydraulic transitions are associated with intense turbulence, is not predicted (Figure 15). The maximum turbulent intensity is only about $\sqrt{K}/U \approx$0.15, and the most intense turbulence is restricted to the most intense shear layer. It turns out that the Gatski- Speziale (1993) modified model predicts the U/NH=0.4- flow almost similarly to the standard model, but the maximum turbulent intensity is now $\sqrt{K}/U \approx$0.2 instead of 0.15. The figures 17 and 18 show that a prediction with stratification effects removed from the turbulence model is significantly different than from these two models. The main reattachment point is now estimated as about $(x_1, x_2)/H \approx$ (5.0, 0) and the width of the recirculating area is limited to $(x_1, x_2)/H \approx$ (2.0, 1.0) (Figures 17 and 18), in better agreement with the data (Hunt and Snyder's 1980 Figure 15b). The turbulence intensity is also much larger, in agreement with common conceptions of such flows. However, since this is a nonstandard turbulence model, it will not be applied further.

The grid dependence of the standard model is simulated on the same grids as illustrated in Figure 6, but it is difficult to characterize this flow in terms of a few variables. Obviously coarse grids cannot resolve the large gradients near the transition and the coarsest grid, $\triangle x_1/H \approx 0.86$, turns out not even to predict the tendency to downslope speedup. Also, since now $\triangle x_1 \approx (\lambda/2)$ (Equation 11), the lee wave pattern is folded to become a more variable and shorter wavelength wake flow than indicated in the Figures 14 and 15. However, at the resolution $\triangle x_1/H \approx 0.43$, both the tendency to downslope jet and the hydraulic transition is predicted (Figure 16). The maximum turbulent intensity turns out to be estimated as $\sqrt{K}/U \approx$0.15 for all reasonable grids, which are probably major underestimates.

Figure 19 illustrate a two-dimensional flow with D/H=1.4 and $U/c_r \approx$0.28 (corresponding to NH/U=2.5), and in agreement with Sheridan and Vosper (2005) and Eidsvik and Utnes (1996), an hydraulic transition is predicted behind the hill. There is a strong downslope wind near the surface with an overturning flow higher and behind (compare Figure 14, 14). The characteristic wavelength for the moderate amplitude waves above the density interface is: $\lambda/D \approx 1.63$, which is more like $\lambda/D \approx 2\pi U/ND \approx$1.78 instead of like $\lambda/D \approx$1.0 from Equation 10. This is physically reasonable since the flow below the density interface do not now participate in the wave flow. Since the lower level flow is neutrally stratified, it is reasonable that the turbulence intensity is now much higher than in Figure 15.

The grid dependence of the flow in Figure 19 is also difficult to characterize in terms of a few variables so that a coarse grid integration is illustrated instead in Figure 20. As indicated by the vorticity distribution, the density interface layer cannot be represented properly on the coarse grid and there is a strong turbulent wake in front of the hill. However, the transition flow behind the hill is estimated even on the coarse grid. The maximum turbulent intensity in this area, which is estimated as $\sqrt{K}/U \approx$0.5 on the most detailed grid, is estimated as high as $\sqrt{K}/U \approx$0.35 even for the coarsest grid, which is comparable to the relative grid variations in figures 8 and 13.

In summary: strongly stratified flows with hydraulic transitions, $U/NH <$0.4, require better turbulence models for accurate predictions. The grid requirements are also stronger than for the other flows discussed. Nevertheless, useful predictions of transitions may be obtained even for $\triangle x_1/H \approx 0.4$ or so. Again it should be recalled that $\triangle x_1/L$ is also supposed to be sufficiently small, say $\triangle x_1/L <$0.2, so that a hydraulic transition can be represented.

4 Concluding Remarks

In neutral- and moderately stratified flows, say for U/NH >0.5 and U/c_r >0.6, the standard (K, ϵ)-model appears to be usefully accurate. Resirculating flows and characteristic lee wavelengths are predicted reasonably accurately even on sparse grids. Lee wave amplitudes are predicted less accurately, particularly so for three-dimensional flows. Provided that the gridding is better than about $\triangle x_1/H$ <0.5 or so, the relative grid error for the turbulence intensity is estimated as: $\delta\sqrt{K}/\sqrt{K}$ <0.25, which is comparable to the large scale error and about as accurate as turbulence models normally can be, particularly so for geophysical flows. For flows with separation or rotor flows, the error is systematic so that if the gridding is comparable to $\triangle x_1/H$ ∼0.5, the turbulent intensity is underestimated with about 25 percent.

In strongly stratified flows, say for U/NH <0.4, usefully accurate predictions of hydraulic transitions may be obtained even for $\triangle x_1/H$ <0.4 or so. However, in such flows any few-equation turbulence model must be considered to be seriously uncertain, and this is also illustrated in the present simulations. Flows with hydraulic transitions are dramatic, but if H is moderate, they are also normally associated with moderate U-values, which give moderate turbulence, so that this is usually not very important for flight safety.

5 References

Baines P.G. (1995): Topographic Effects in Stratified Flows. Cambridge Monographs on Mechanics. 1995 482 pp

Brørs B., Eidsvik K.J. (1992): Dynamic Reynolds Stress Modelling of Turbidity Currents. Journal of Geophysical Research Vol 97 C6 pp 9645–9652

Brørs B., Eidsvik K.J. (1992): Oscillatory boundary layer flow modelled with Reynolds Stress turbulence closure. Continental Shelf Rearch Vol 33 pp 219–242

CastroF.A., Palma J.M.L.M., Silva Lopes A. (2003): Simulations of the Askervein Flow. Part 1 Reynolds Average Navier-Stokes equations (k-ϵ turbulence model) Boundary-Layer Meteorology 2003, Vol 40 pp 1-29

Clark T.L., Keller T., Coen J., Neilley P., Hsu H.-M., Hall E.D. (1997): Terrain-Induced Turbulence over Lantau Island: 7 June 1994 Tropical Storm Russ Case Study. J. Atmos. Sci. Vol 54 pp 1795–1814

Eidsvik K.J., Utnes T. (1997): Flow separation and hydraulic transition over hills modelled by the Reynolds equations. Journal of Wind engineering and industrial aerodynamics. Vol 67+68 pp 403-413

Eidsvik K.J., Holstad A., Lie I., Utnes T. (2004): A Prediction System for Local Wind Variations in Mountainous Terrain. Boyndary-Layer Meteorology Vol 112 pp 557–586

Eidsvik K.J.(2005): A system for Wind Power Estimation in Mountainous Terrain. Prediction of Askervein Hill Data. Wind Energy Vol 8 pp 337–249

Gatski T.B., Yousuff Hussaini M., Lumley J.L. (1996): Simulation and Modeling of Turbulent Flows. ICASE/LaRC Series in Computational Science and Engineering.Oxford University Press.

Emanuel K.A. (1994): Atmospheric Convection. Oxford University Press pp 570

Kaimal J. C., Finnigan J. J. (1994): Atmospheric Boundary Layer Flows. Their Structure and Measurement. Oxford University Press.

Kalnay E. (2002): Atmospheric modeling, data assimilation and predictability. Cambridge university press. 341 pp

Jackson P.S., Hunt J.C.R. (1975): Turbulent flow over a low hill. Quart.J. R. Met Soc. Vol 101 pp 929–955

Hewitt G.F., Vassilicos J.C. (2005): Prediction of turbulent Flows. Cambridge Unuversity Press 343 pp

Hunt J.C.R., Snyder W.H. (1980): Experiments on stably and neutrally stratified flow over a model three-dimensional hill. Journal of Fluid Mechanics. Vol 96 pp 671–704

Lie I., Utnes T., Blikberg R. (2003). On preconditioned iterative solution of distributed sparse linear systems in SIMRA. *http://balder.ntnu.no/ttp*

Lindborg E., Cho J.Y.N. (2001) Horizontal velocity structure functions in the upper troposphere and lower stratosphere. ". Theoretical considerations. Journal of geophysical research Vol 106 no D10. pp 10233–10241

Panofsky H.A.and Dutton J.A. (1985): Atmospheric Turbulence.John Wiley,New York. 397pp.

Pope S.B. (2000): Turbulent Flows Cambridge University Press 771 pp

Rodi W., Bonnin J.C. (1997): 6th EUROFAC/IAHR/COST/Workshop on refined Flow modelling, June 1997, TU Delft, The Netherlands. http://tmbd.ws.tn. tudelft.nl/workshop6.html

Utnes T., Eidsvik K.J. (1996): Turbulent flows over mountains modelled by the Reynolds equations. *Boundary-Layer Meteorology. Vol 79 pp 393-416*

Utnes T. (2002). Numerical formulation of a semi-implicit Reynolds-averaged model (SIMRA). *SINTEF Applied Mathematics 2002. http://balder.ntnu.no/ttp*

Wurtele M.G., Sharman R.D., Datta A. (1996): Atmospheric Lee Waves. Annual review of Fluid Mechanics. Vol 28 pp 389–428

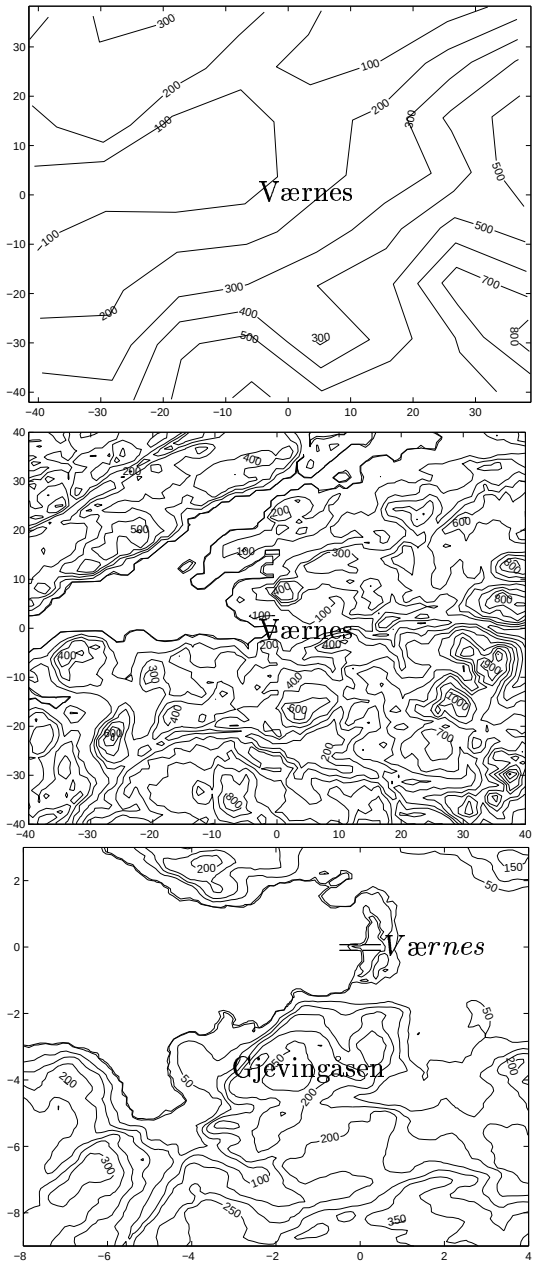

HIRLAM, hydrostatic weather prediction model. Contains estimated and forecasted large scale flow. Near ground resolution: $(\triangle x_1, \triangle x_3) \approx$ (10 km, 50 m)
Provides boundary conditions for UM
$\Downarrow$

UM, non-hydrostatic. Near ground resolution: $(\triangle x_1, \triangle x_3) \approx$(1 km, 20 m)
Provides boundary conditions for SIMRA

$\Downarrow$

SIMRA, non-hydrostatic. Near ground resolution: $(\triangle x_1, \triangle x_3) \approx$(100 m, 1 m)
Contains predicted local flow

Figure 1: Prediction system for local flow illustrated by the representation of the topography in the different models (Eidsvik et al 2004). The HIRLAM topography is only shown over the integration domain of the UM model, illustrated in the middle panel. Coordinates in km. Except for the two isolines applied for contouring the sea-shore, the height isoline increment are 100m in the two first figures and 50m in the last. Værnes airport is indicated in each panel. The Gjevingåsen hill is about 300 m high.

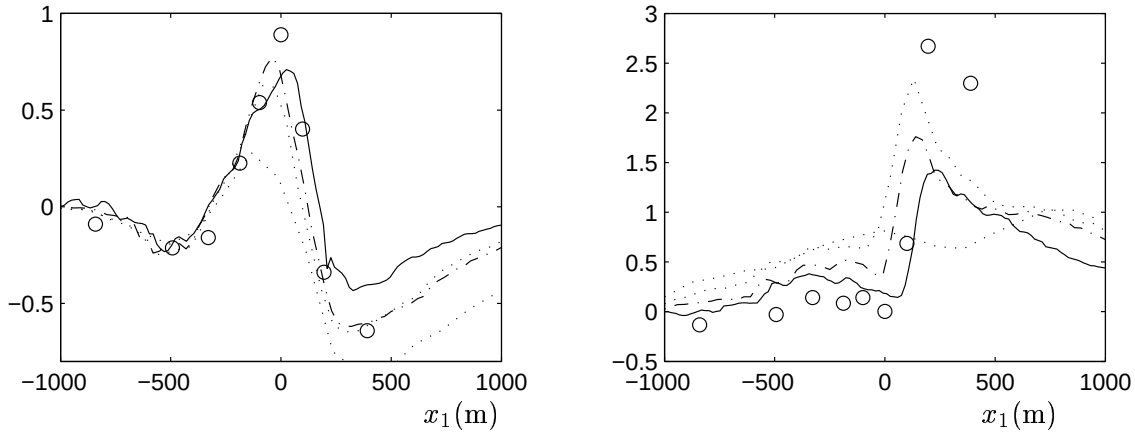

[h!]

Figure 2: Predicted and measured flow over the Askervein AA-profile in (m) a): $\triangle u/u_0$, b): $\triangle K/K_0$. Integration domain: $x_i/H \in$(-6,15),(-6,6), (0,5), and different grid resolutions: —-: $\triangle x_1/H$=0.19, ($N_1 \times N_2 \times N_3 = 125 \times 125 \times 65$) -.-.: $\triangle x_1/H$=0.35, ($N_1 \times N_2 \times N_3 = 69 \times 69 \times 41$). ....: $\triangle x_1/H$=0.61, ($N_1 \times N_2 \times N_3 = 39 \times 39 \times 21$) ....: $\triangle x_1/H$=1.41, ($N_1 \times N_2 \times N_3 = 17 \times 17 \times 11$).(Compare Eidsvik 2005)

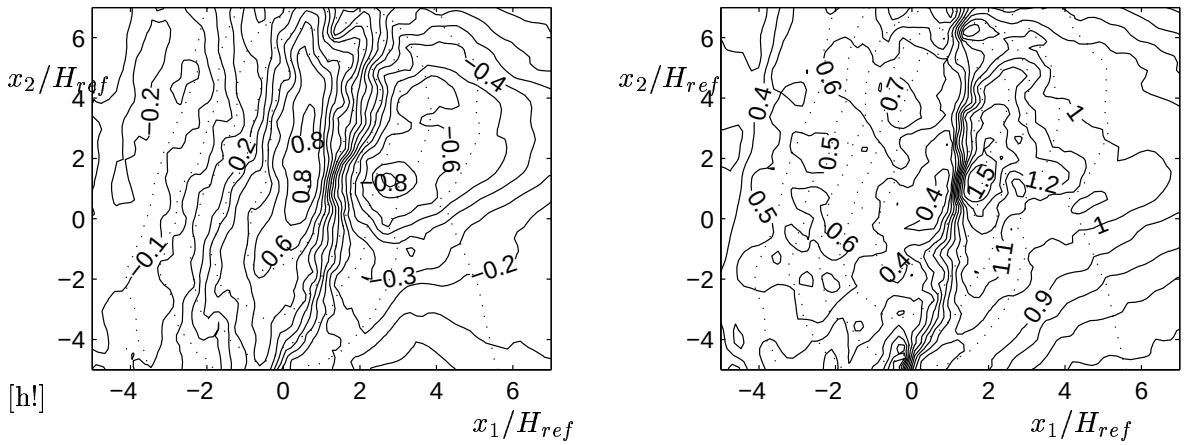

[h!]

Figure 3: As in Figure 2 except coordinates in x_i/H_{ref}, H_{ref}=121m and: a): $\triangle u/u_0$ 10 m above the terrain. b): $\triangle K/K_0$ 10 m above the terrain. The AA-profile crosses the hilltop at (x_1, x_2)=(0,0) with an angle of -15 deg.

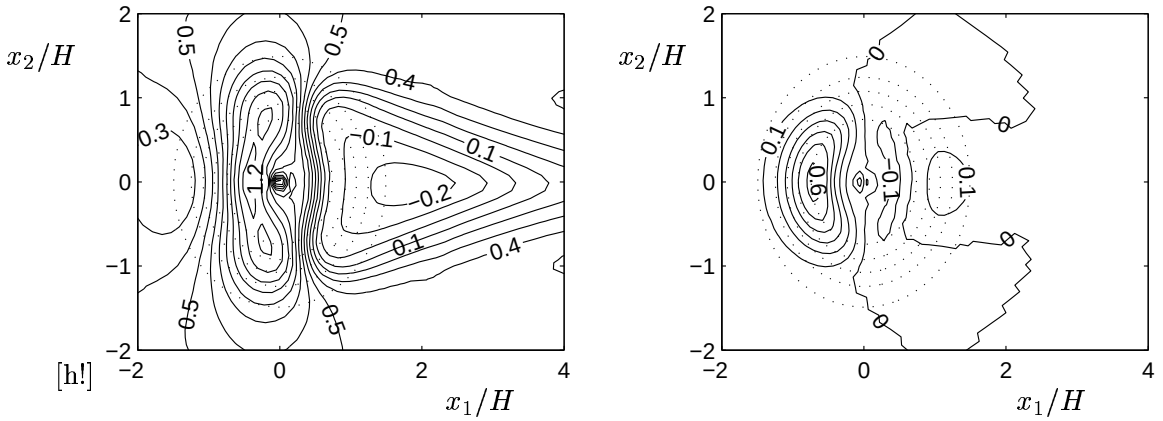

[h!]

Figure 4: Neutrally stratified flow over the Hunt Snyder (1980) hill-shape H=500m, D=150m, z_0=0.165m, U=10 m/s. Estimated flow at 10m height above the terrain a): u_1/U b): u_3/U. $\triangle x_1/H \approx 0.12$, Integration domain: $x_i/H \in$=(-5,15),(-5,5), (0,5), $(N_1 \times N_2 \times N_3 = 137 \times 111 \times 71)$.

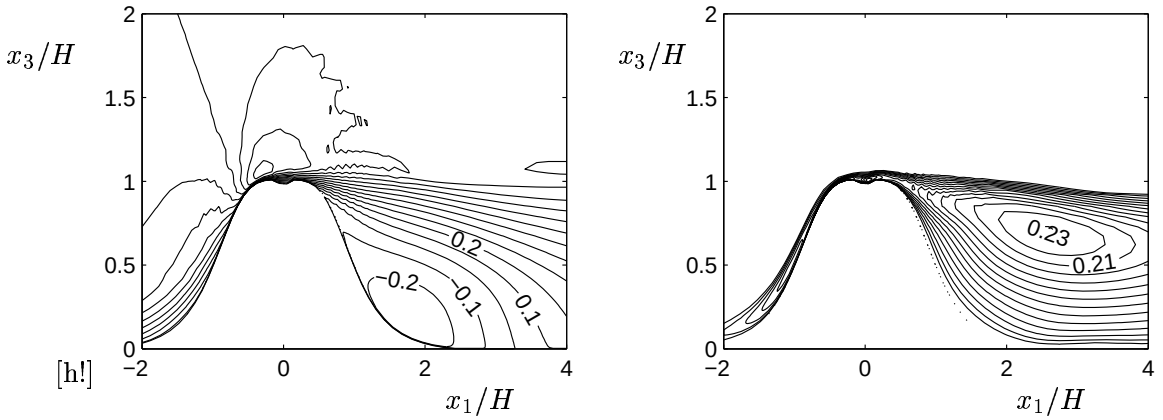

[h!]

Figure 5: As in Figure 4 except vertical cross section over the hilltop. a) Horizontal velocity component u_1/U, b) Turbulent intensity $\sqrt{K}/U$.

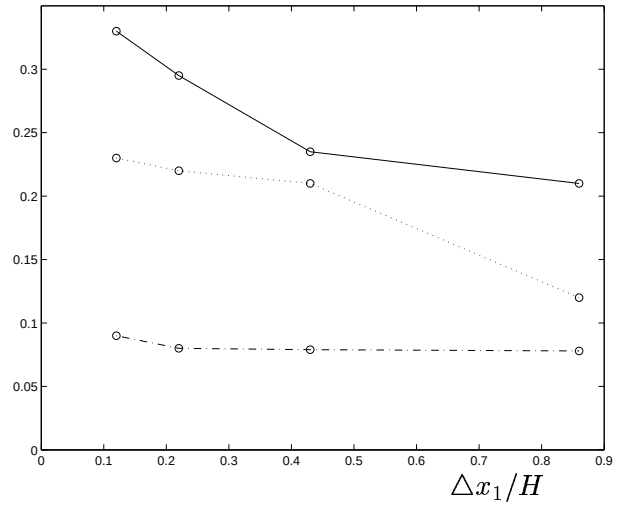

[h!]

Figure 6: Flow and simulations like in Figure 4. Reattachment distance $(x_r/H)/10$——, Width of reattachment area $(y_r/H)/10$-.-. Maximum turbulent intensity $\sqrt{K}/U$..... as functions of grid resolution $\triangle x_1/H$. Grids: $(N_1 \times N_2 \times N_3) = (137 \times 111 \times 71)$, $(71 \times 61 \times 41)$, $(37 \times 31 \times 21)$, $(19 \times 15 \times 11)$

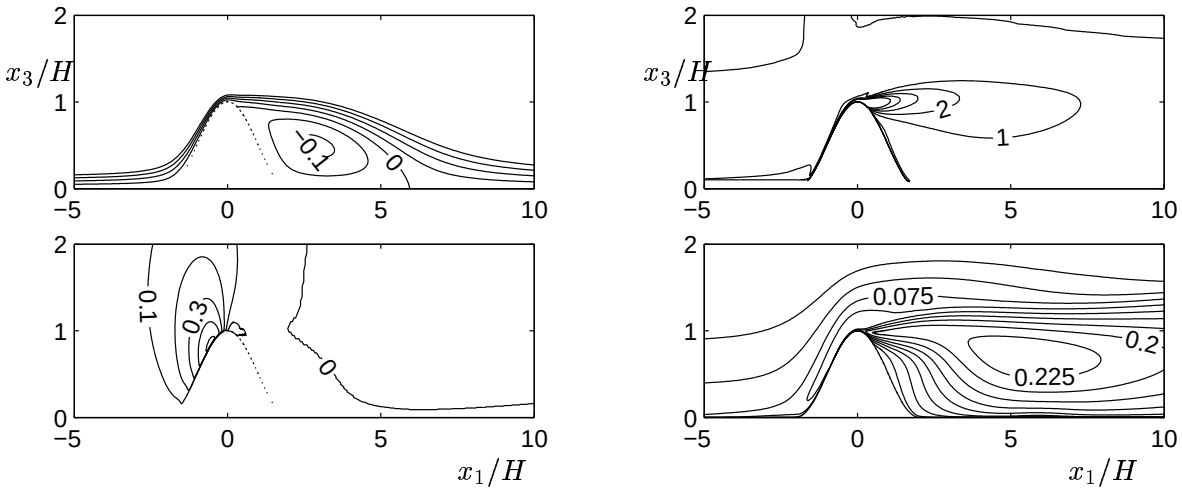

Figure 7: Predicted neutrally stratified flow over a two-dimensional cosine-square hill with $L/H = 2$ Grid resolution: $\triangle x_1/H$=0.052, corresponding to $N_1 \times N_2 \times N_3 = 401 \times 3 \times 121$. Integration domain: x_i/H $\in$=(-6,15),(-0.1,0.1), (0,5). Row-wise: a) Streamlines ψ/HU, b) Vorticity $\omega_2 H/U$, c) Vertical velocity component u_3/U, d) Turbulent intensity $\sqrt{K}/U$.

[h!]

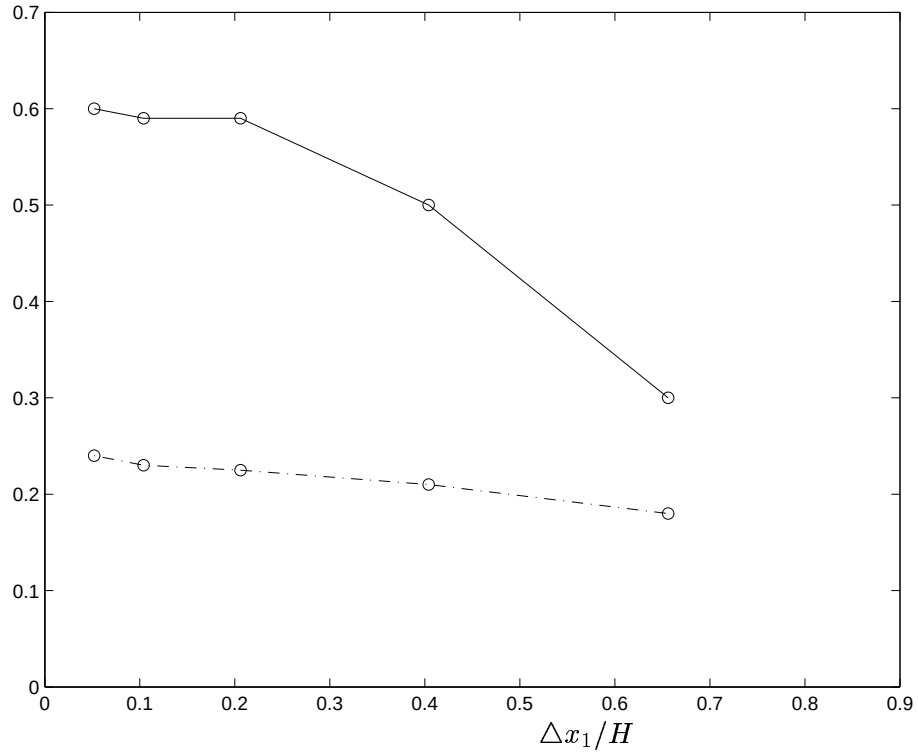

Figure 8: Flow and simulations like in Figure 7. Reattachment distance $(x_r/H)/10$—– and maximum turbulent intensity $\sqrt{K}/U$-.-. as functions of grid resolution $\triangle x_1/H$. Grids: $(N_1 \times N_2 \times N_3) = (401 \times 3 \times 121)$, $(201 \times 3 \times 101)$, $(101 \times 3 \times 51)$, $(31 \times 3 \times 15)$

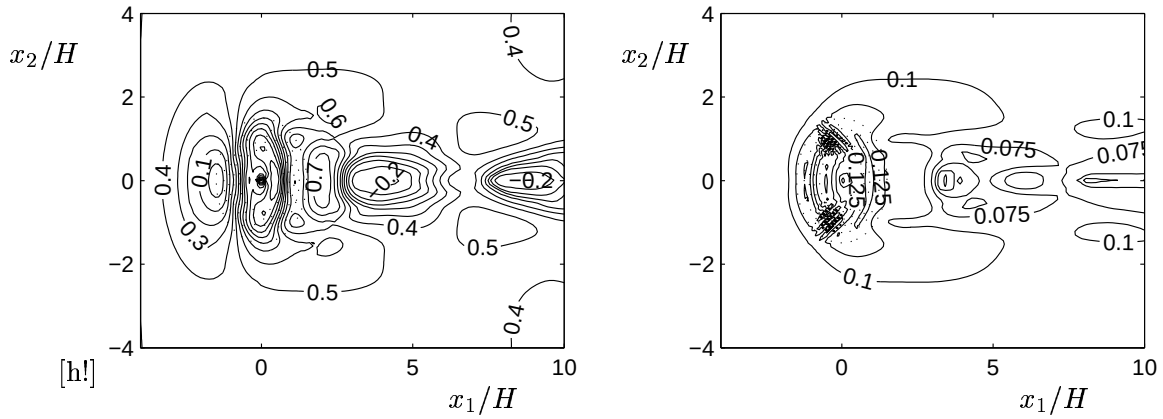

[h!]

Figure 9: Stratified flow (F=U/NH=0.8) over the Hunt Snyder (1980) hill-shape H=500m, D=150m, z_0=0.165m, U=10 m/s. Estimated flow at 10m height above the terrain a): u_1/U b): u_3/U. Wake isolines are for many similar small values. Integration domain: $x_i/H \in$=(-5,15),(-5,5), (0,5), $\triangle x_1/H \approx 0.12$, ($N_1 \times N_2 \times N_3 = 137 \times 111 \times 71$).

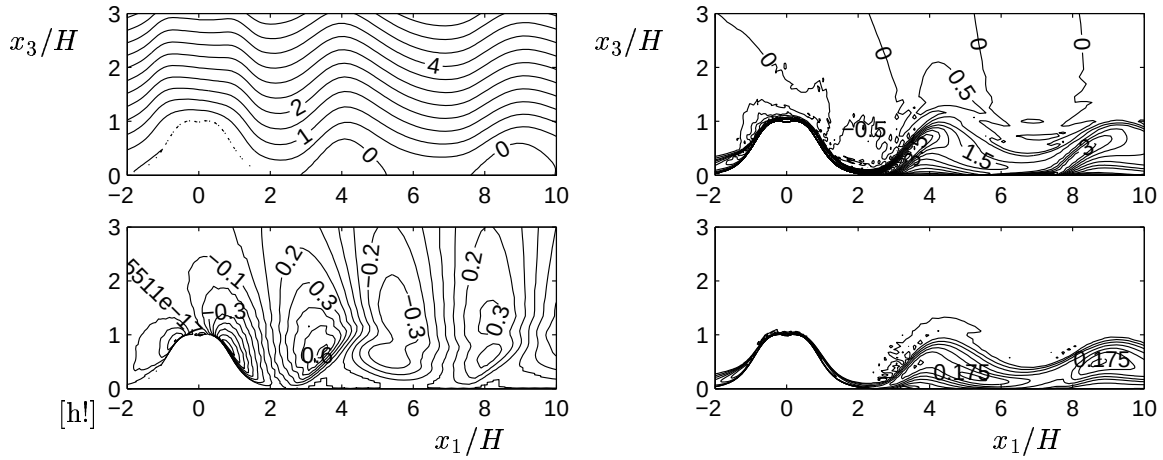

[h!]

Figure 10: As in Figure 9 except vertical cross sections. Rowwise: a) Streamlines ψ/HU, b) Vorticity $\omega_2 H/U$, c) Vertical velocity u_3/U, d) Turbulent intensity $\sqrt{K}/U$.

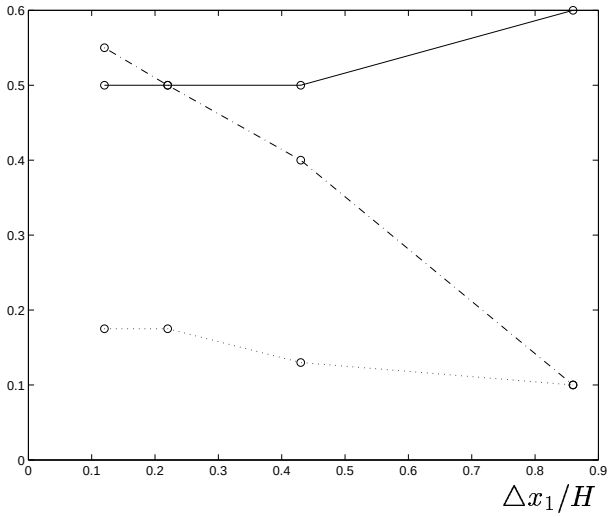

Figure 11: Flow and simulations like in Figure 9. Characteristic wavelength $(\lambda/H)/10$——, Maximum lee wave vertical velocity u_3/U-.-. Maximum turbulent intensity $\sqrt{K}/U$..... as functions of grid resolution $\triangle x_1/H$. Grids: $(N_1 \times N_2 \times N_3) = (137 \times 111 \times 71)$, $(71 \times 61 \times 41)$, $(37 \times 31 \times 21)$, $(19 \times 15 \times 11)$

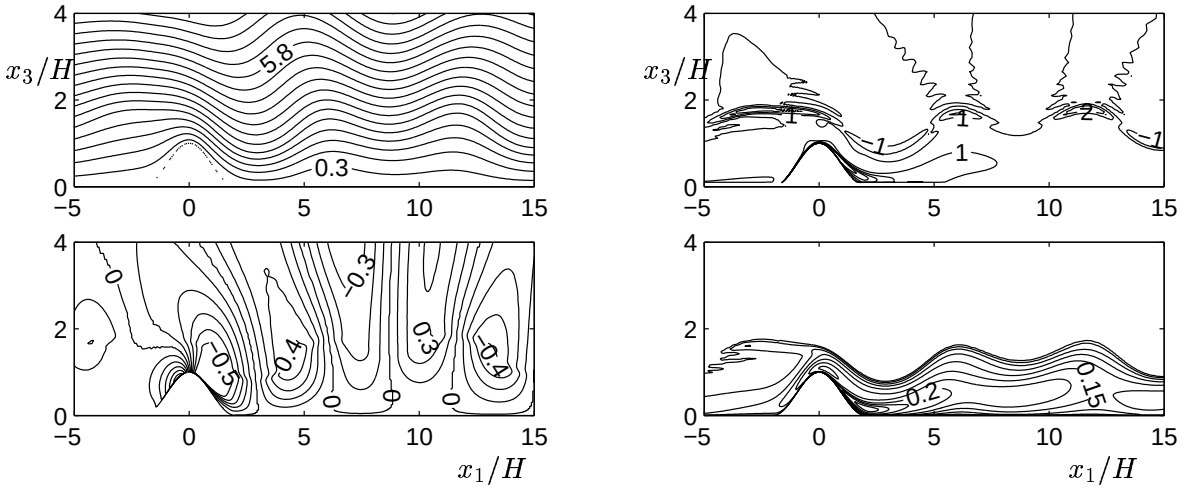

Figure 12: As in Figure 7 except stratified flow above D/H= 1.4, Inversion of $\triangle\theta$=8.4 C and ND/U=1 above. U/c_r=0.67 Integration domain: x_i/H $\in$=(-6,20),(-0.1,0.1), (0,7). $\triangle x_1/H$ =0.065 corresponding to: $N_1 \times N_2 \times N_3 = 401 \times 3 \times 121$.

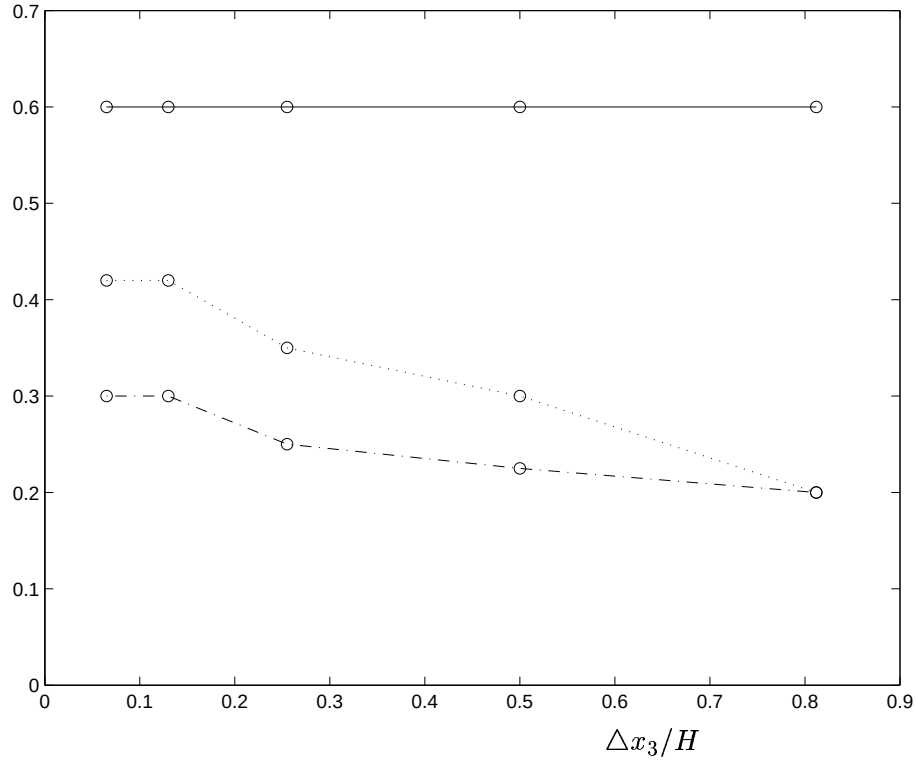

[h!]

Figure 13: Flow and simulations like in Figure 12. Characteristic wavelength $(\lambda/H)/10$—– , maximum turbulent intensity $\sqrt{K}/U$-.-. and typical maximum wave vertical velocity u_3/U..... as functions of grid resolution $\triangle x_1/H$. Grids: $N_1 \times N_2 \times N_3 = 401 \times 3 \times 121$, $201 \times 3 \times 101$, $101 \times 3 \times 51$, $31 \times 3 \times 15$

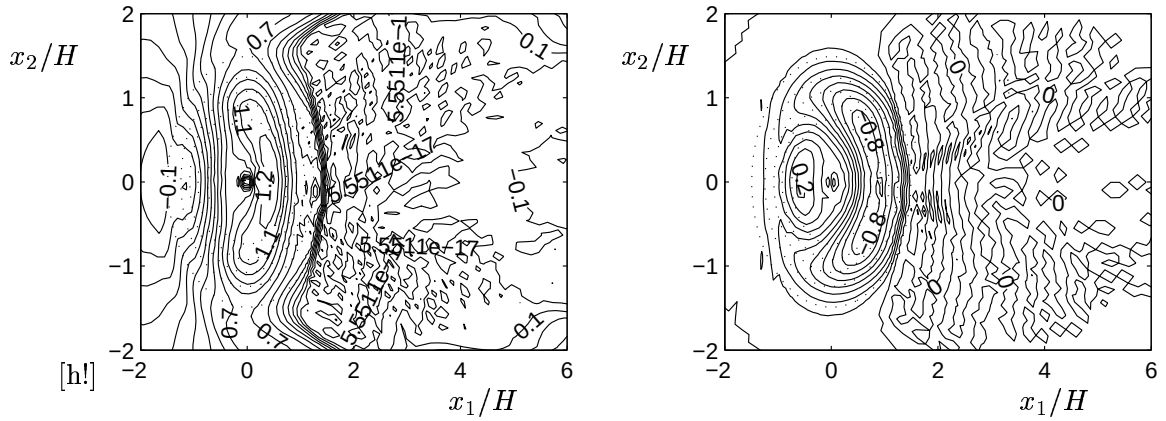

[h!]

Figure 14: Stratified flow (F=U/NH=0.4) over the Hunt Snyder (1980) hill-shape H=500m, D=150m, z_0=0.165m, U=10 m/s. Estimated flow at 10m height above the terrain a): u_1/U b): u_3/U. Wake isolines are for many similar small values. Integration domain: $x_i/H \in$=(-5,15),(-5,5), (0,5), $\triangle x_1/H \approx 0.12$, ($N_1 \times N_2 \times N_3 = 137 \times 111 \times 71$).

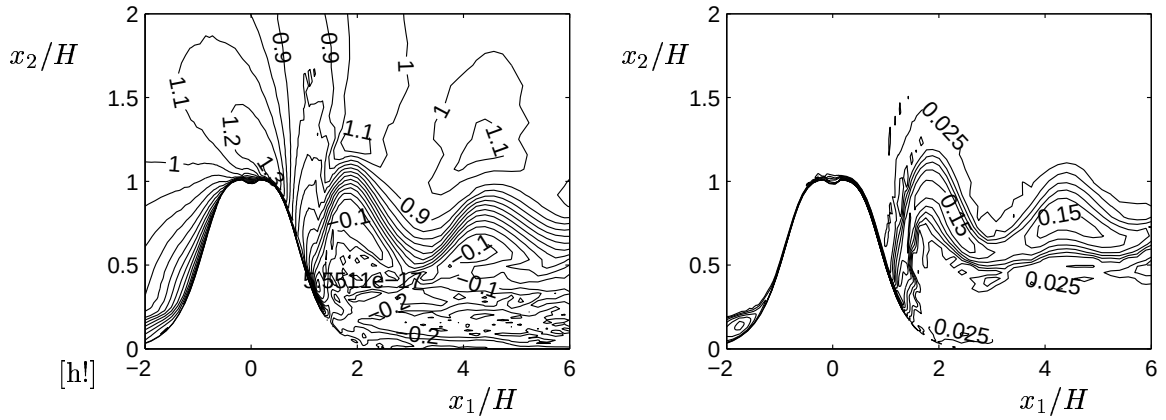

[h!]

Figure 15: As in Figure 14 except vertical cross section over the hilltop. a) u_1/U b) Turbulent intensity $\sqrt{K}/U$.

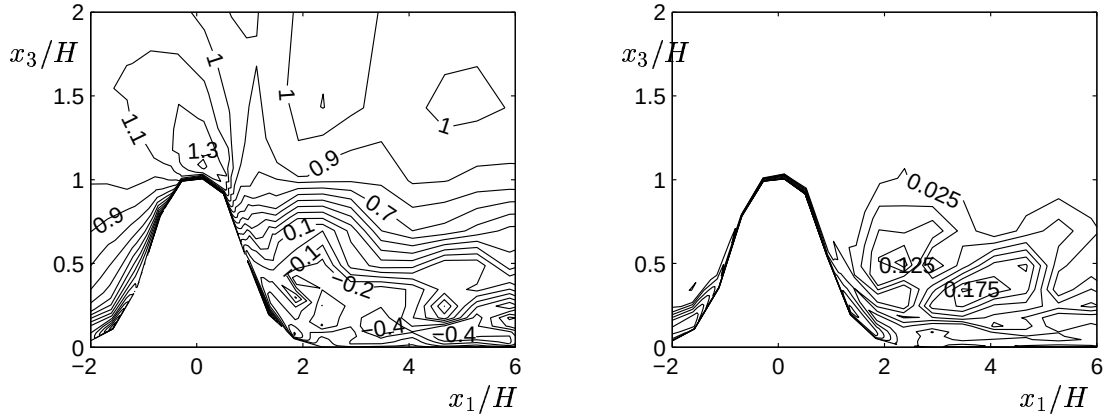

Figure 16: As in Figure 15 except $\triangle x_1/H \approx 0.43$, ($N_1 \times N_2 \times N_3 = 37 \times 31 \times 21$)

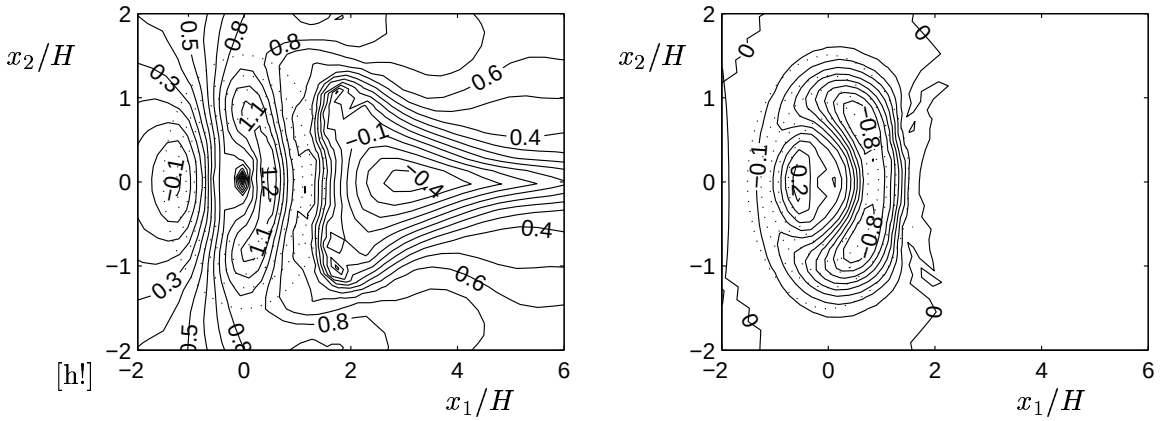

[h!]

Figure 17: As in Figure 14 except turbulence model without stratification effects. a): u_1/U b): u_3/U. $\triangle x_1/H \approx 0.22$, $(N_1 \times N_2 \times N_3 = 72 \times 61 \times 41)$.

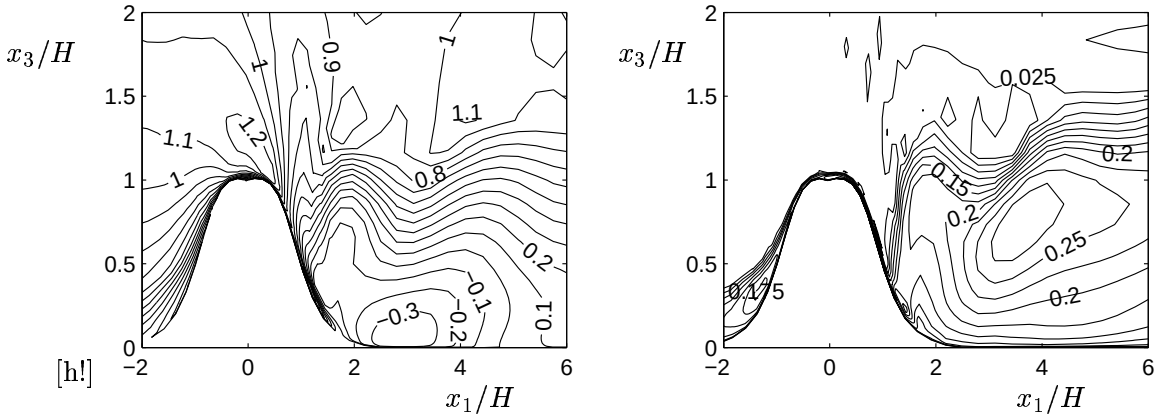

[h!]

Figure 18: As in Figure 17 except vertical cross section over the hilltop. a) u_1/U b) $\sqrt{K}/U$.

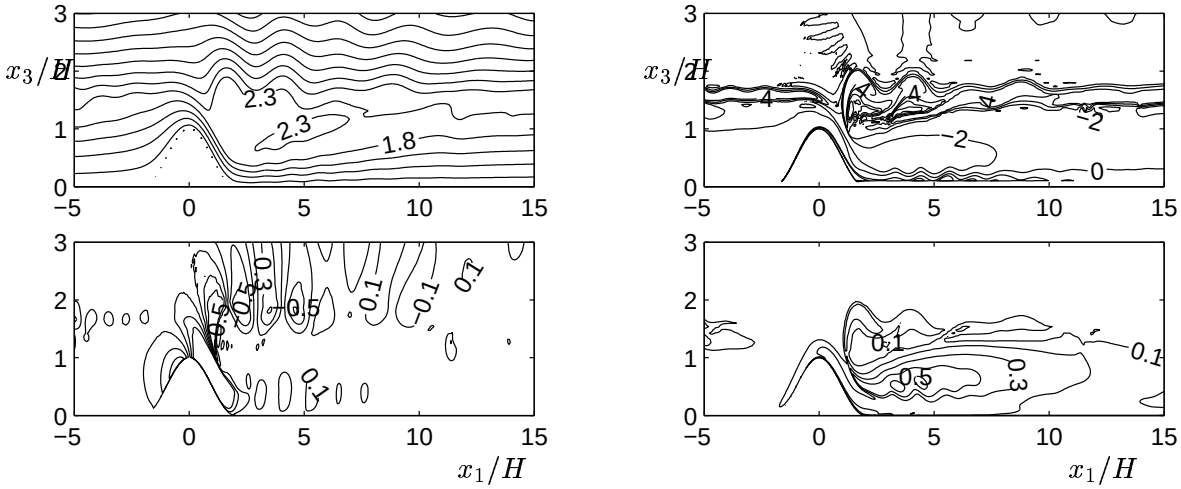

Figure 19: As in Figure 12 except U/c_r=0.28

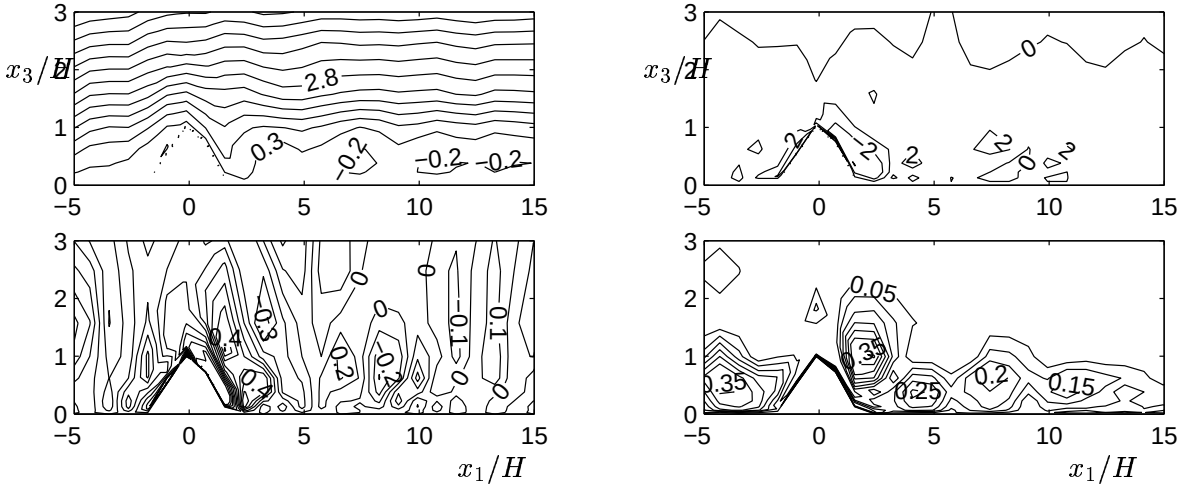

Figure 20: As in Figure 19 except $\triangle x_1/H$= 0.81, corresponding to: $N_1 \times N_2 \times N_3 = 31 \times 3 \times 15$